International Journal of Energy Production and Management
https://www.acadlore.com/journals/IJEPM

Development of a Photoelectrochemical Cell for Hydrogen Production

Sunday A. Afolalu[1,2,3], Temitayo S. Ogedengbe[2,3,4*], Emmanuel F. Lawal[1], Tin T. Ting[3]

[1] Department of Mechanical and Mechatronics Engineering, Afe Babalola University, 360101 Ado Ekiti, Nigeria
[2] Department of Mechanical Engineering Science, University of Johannesburg, 2092 Johannesburg, South Africa
[3] Faculty of Data Science and Information Technology, INTI International University, 71800 Putra Nilal, Malaysia
[4] Department of Mechanical Engineering, Nile University of Nigeria, 900001 Abuja, Nigeria

[*] Correspondence: Temitayo S. Ogedengbe (temitayo.ogedengbe@nileuniversity.edu.ng)

Received: 10-09-2025 **Revised:** 12-05-2025 **Accepted:** 12-11-2025

Citation: S. A. Afolalu, T. S. Ogedengbe, E. F. Lawal, and T. T. Ting, "Development of a photoelectrochemical cell for hydrogen production," *Int. J. Energy Prod. Manag.*, vol. 11, no. 1, pp. 77–88, 2026. https://doi.org/10.56578/ijepm110106.

Abstract: This study presents the development and performance evaluation of a photoelectrochemical (PEC) cell designed for sustainable hydrogen production, emphasizing a cost-effective and reproducible approach to clean energy generation. The PEC system was fabricated using an n-type TiO_2 photoanode and Pt cathode in an aqueous Na_2SO_4 electrolyte (0.5 M), operating under simulated solar irradiation of 100 mW/cm^2 (AM 1.5 G) within a controlled temperature range of 25–45 ℃. Experimental testing demonstrated that the system sustained hydrogen evolution through an automated electrolyte refilling and pump control mechanism, achieving 51% H_2 saturation within an average of 2.8 seconds over 172 activation cycles, indicating responsive system logic. However, prolonged operation led to efficiency decline, with pump activation time extending to 833 seconds and only 56% hydrogen recovery, signifying material and control degradation. The temperature monitoring subsystem malfunctioned, registering persistent –127 ℃ readings, which impeded accurate thermal regulation and safety evaluation. Sensor drift and inconsistent pump actuation were also observed, reflecting calibration deficiencies. Three operational phases were identified—initial instability (0–300 s), stabilization (300–600 s), and performance degradation ($\geq$800 s). Overall, while the PEC system demonstrates promising short-term hydrogen generation efficiency under defined light and electrolyte conditions, long-term stability remains constrained by electrode durability, thermal control accuracy, and system integration challenges, requiring further optimization for sustained hydrogen production.

Keywords: Control system reliability; Energy efficiency; Hydrogen production; Renewable energy; Sensor calibration; System integration

1 Introduction

The increasing global concern over climate change has intensified the demand for sustainable and low-carbon energy systems. Fossil fuel combustion remains the dominant contributor to greenhouse gas emissions, driving the urgent transition toward cleaner energy alternatives [1]. Among the available options, hydrogen has emerged as a promising energy carrier due to its high energy density, environmental compatibility, and zero-carbon emissions during utilization in fuel cells. When produced through renewable means, hydrogen offers a viable pathway to decarbonize power generation, transportation, and industrial sectors (Figure 1) [2, 3].

Within this context, photoelectrochemical (PEC) water splitting has gained attention as a highly promising route for renewable hydrogen generation. Unlike conventional electrolysis, PEC systems directly convert solar energy into chemical energy by harnessing semiconductor photoelectrodes to generate electron–hole pairs that drive redox reactions, splitting water into hydrogen and oxygen without producing harmful by-products [4, 5]. The overall efficiency of a PEC cell depends on several interrelated factors, including light absorption capability, charge carrier separation efficiency, and the long-term stability of the photoelectrode materials [6, 7].

Advances in materials science and nanotechnology have led to notable improvements in PEC performance through techniques such as bandgap engineering, surface modification, and heterojunction design [8, 9]. Despite these gains, persistent challenges remain—particularly with respect to achieving long-term material stability, reducing

fabrication costs, and enhancing solar-to-hydrogen conversion efficiency. Moreover, the transition from laboratory-scale prototypes to commercially viable PEC systems necessitate scalable, low-cost manufacturing approaches and robust materials capable of maintaining efficiency under continuous operational stress [10, 11].

However, most existing studies primarily focus on improving conversion efficiency while often neglecting critical aspects such as operational reliability, sensor accuracy, and control system performance under real-world conditions [11]. Addressing these gaps requires a holistic design approach that integrates material optimization, efficient control logic, and cost-effective fabrication. Therefore, this study develops and evaluates a high-performance, low-cost PEC cell for hydrogen generation, with emphasis on sustained operation and system reliability. The findings contribute to advancing practical, scalable solutions for solar-driven hydrogen production, supporting the global transition toward a cleaner and more resilient energy future [12].

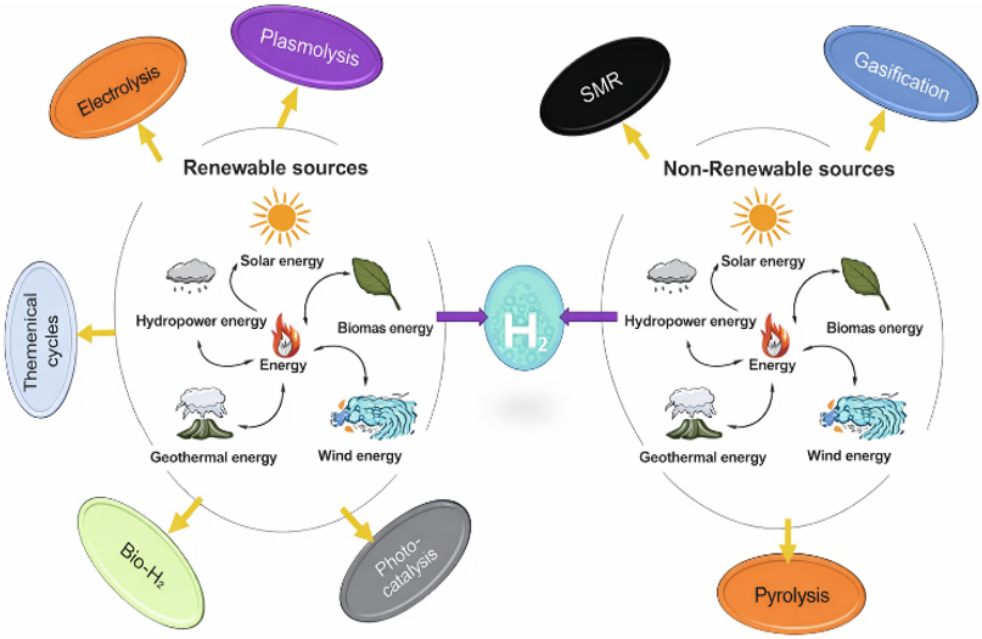

Figure 1. Renewable and non-renewable energy cycle and sources [3]

2 Literature Review

Hydrogen production via PEC water splitting has gained considerable attention for its potential to directly convert solar energy into sustainable fuel [4]. Since the pioneering work of Fujishima and Honda in 1972, who first demonstrated water splitting using TiO_2 under ultraviolet illumination, significant progress has been achieved in understanding semiconductor photoelectrodes and improving solar-to-hydrogen (STH) conversion efficiencies [5, 13]. A PEC system operates by using semiconductor materials to absorb photons, generating charge carriers that drive hydrogen and oxygen evolution reactions at the electrode–electrolyte interface [6]. Figure 2 shows examples of semiconductor materials for PEC systems. Despite decades of progress, achieving high efficiency, long-term stability, and cost-effectiveness under real-world conditions remains a major challenge. Figure 3 shows the flow of electrodes from photoanode in a PEC cell.

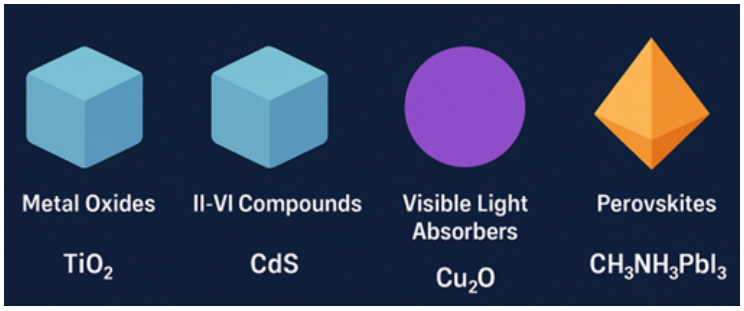

Figure 2. Semiconductor materials for photoelectrochemical (PEC) systems

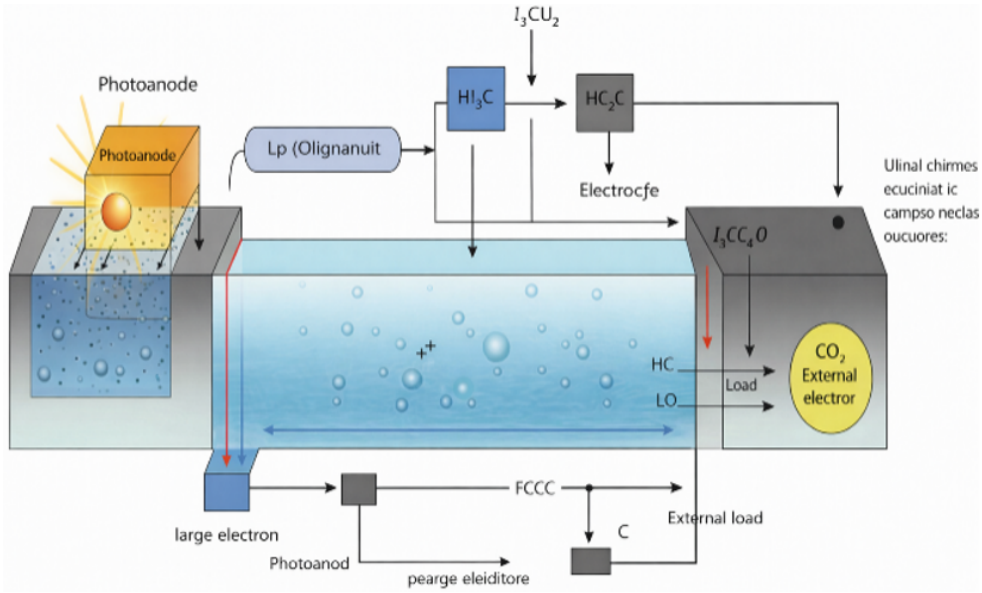

Figure 3. Photoelectrochemical (PEC) cell [5]

2.1 Semiconductor Materials for Photoelectrochemical Systems

The semiconductor photoelectrode forms the foundation of PEC cell performance. Metal oxides such as TiO_2, Fe_2O_3, and WO_3 have been widely studied due to their chemical stability, abundance, and low cost [2]. However, their wide band gaps (2.6–3.2 eV) restrict absorption to the ultraviolet spectrum, which represents less than 5% of solar radiation. To overcome this limitation, research has expanded toward narrow-bandgap semiconductors such as CdS, Cu_2O, $BiVO_4$, and perovskite-based materials, which exhibit enhanced visible-light absorption and improved STH efficiency [3, 9].

Further progress has been achieved through nano structuring, doping, and heterojunction engineering. For example, TiO_2/Fe_2O_3 and $BiVO_4/WO_3$ heterojunctions improve interfacial charge transfer, while dopants such as nitrogen, sulfur, and transition metals tailor the band structure to reduce recombination losses [7, 10, 14–16]. Nevertheless, most semiconductors still suffer from photoelectrode instability and photo corrosion under prolonged operation, which significantly limits their durability in practical systems.

2.2 Catalyst and Electrode Surface Engineering

Efficient catalytic surfaces are critical to enhance the kinetics of the hydrogen and oxygen evolution reactions. While noble metals such as Pt, RuO_2, and IrO_2 remain the most active catalysts, their scarcity and high cost hinder large-scale deployment [1]. Consequently, recent studies have explored earth-abundant alternatives such as Ni, Co, MoS_2, and transition metal phosphides, which offer promising catalytic performance with improved stability [8].

Surface engineering techniques—including atomic layer deposition (ALD), electrochemical etching, and hydrothermal growth—have been employed to increase active surface area and improve charge transport [9]. Protective coatings such as TiO_2 or Al_2O_3 further mitigate photo corrosion and extend photoelectrode lifespan under illumination [17]. Despite these advancements, the combined optimization of catalyst integration and semiconductor stability remains an open research area, particularly under sustained solar operation.

2.3 Photoelectrochemical Cell Configuration and System Optimization

Beyond material development, overall PEC cell architecture and system control play crucial roles in determining performance. Conventional single-junction PEC cells often exhibit low efficiency due to incomplete light absorption and charge recombination [6]. Tandem (dual-absorber) systems that combine photoanodes and photocathodes with complementary bandgaps have demonstrated higher conversion efficiencies [2, 18]. Moreover, coupling PEC systems with photovoltaic (PV) modules or applying external bias can enhance STH efficiency beyond 10% [3].

However, system-level challenges persist. Stable hydrogen generation requires effective control of parameters such as electrolyte flow, temperature, and gas collection. Only a few studies have investigated real-time monitoring and feedback control strategies to maintain operational stability under fluctuating sunlight and environmental conditions [4, 19]. The lack of integrated system control remains a bottleneck in transitioning PEC systems from laboratory prototypes to scalable, field-deployable technologies.

2.4 Research Gaps and Current Focus

Based on the reviewed literature, three major research gaps are identified:

• Photoelectrode durability–Existing semiconductors exhibit photocorrosion and degradation under long-term illumination, limiting device lifespan.

• Integrated system control–Few studies have incorporated automated feedback or real-time monitoring to ensure operational stability under varying environmental conditions.

• Scalable, low-cost design–Most laboratory systems remain expensive or complex, with limited demonstration of cost-effective configurations suitable for continuous hydrogen production.

To address these challenges, this study focuses on developing a cost-effective and durable PEC cell with enhanced control reliability and stable hydrogen generation. The proposed system integrates optimized semiconductor materials, effective catalyst interfaces, and automated control logic to improve operational stability and performance. This approach aims to advance practical PEC technology for sustainable hydrogen production, contributing to the global transition toward a low-carbon energy future [10, 20–24].

3 Methodology

3.1 Photochemical Reaction System Design

(a) The photochemical reaction system was designed to enable stable and efficient PEC hydrogen generation by integrating solar power, optimized electrode architecture, and controlled illumination. It consists of four performance-critical subsystems—solar energy supply and storage, electrode assembly, light simulation, and automated illumination control—each configured to ensure continuous operation and consistent hydrogen output.

The solar power subsystem supplied stable electrical energy to the control board and electrolyte pump, ensuring uninterrupted PEC operation. A 250 W monocrystalline panel (17–19% efficiency) tilted 15° southward harnessed peak irradiance of 1000 W/m^2 typical of Nigeria's climate. Two 12 V, 7.5 Ah lead-acid batteries connected in parallel provided a regulated 12 V, 15 Ah output through a PWM controller, maintaining continuous operation under low-light conditions.

The PEC cell employed a titanium dioxide (TiO_2) mesh photoanode for its strong photoactivity, corrosion resistance, and stability in alkaline media. The mesh geometry increased light absorption and surface area, improving charge transfer efficiency. A graphite rod, repurposed from a dry cell, served as the cathode due to its high conductivity and chemical inertness. Potassium hydroxide (KOH) acted as the electrolyte, enhancing ionic conductivity and supporting the oxygen and hydrogen evolution reactions. This TiO_2–graphite–KOH configuration provided a cost-effective and durable setup for efficient hydrogen generation.

Controlled illumination was achieved through a customized light simulation unit consisting of 24 V broad-spectrum LED strips (400–700 nm) arranged in a three-array configuration along the sidewalls and rear panel of the reaction chamber. This configuration was designed to provide uniform light distribution and effective stimulation of TiO_2's photocatalytic activity.

To verify the uniformity of illumination, irradiance mapping was conducted on the electrode plane using a calibrated TES 1339R lux meter (±2% accuracy). Measurements were taken at nine grid points (3 × 3 array) covering the full illuminated area. The recorded intensities ranged between 95 and 101 mW/cm^2, with an average of 98 mW/cm^2 and a maximum deviation of 4.1%, confirming near-uniform exposure across the electrode surface. An LDR-based relay control circuit automatically regulated the lighting system, activating it under low ambient light ($<$200 lux) and deactivating it during adequate daylight to conserve energy. Sensitivity calibration using an onboard potentiometer allowed precise adjustment of switching thresholds, ensuring consistent irradiance during PEC operation.

Overall, the integrated system design combined renewable energy harvesting, efficient electrode materials, and adaptive illumination control to create a reliable and sustainable platform for PEC hydrogen production under both natural and simulated lighting conditions.

3.2 Electronic Control System Design

The system control and hydrogen monitoring framework was designed to enable safe, automated, and data-driven operation of the PEC hydrogen production unit. It integrates real-time gas detection, sensor feedback, and microcontroller-based control logic to maintain operational stability, prevent safety hazards, and facilitate performance evaluation.

The MQ-2 gas sensor was selected for hydrogen detection due to its broad sensing range (300–10,000 ppm), low cost, and reliability. Operating on a tin dioxide (SnO_2) semiconductor, its conductivity varies with hydrogen concentration, enabling quantitative gas estimation. The sensor was preheated for 24 hours and calibrated against known hydrogen concentrations to ensure accurate ppm correlation. Positioned above the reaction chamber for early leak detection, it interfaced with an Arduino Nano microcontroller managing water level and temperature sensors

(I^2C-based), SD card data logging, and relay-driven pump control. Real-time system data were displayed via a serial LCD module.

The Arduino Nano (ATmega328P) functioned as the central control unit owing to its compact architecture, 16 MHz clock speed, and multiple I/O interfaces (I^2C, SPI, UART). Powered by a regulated 5 V supply from the 12 V battery bank, it provided stable and noise-free operation for all connected sensors. The control firmware, written in C++ using the Arduino IDE, implemented a real-time data acquisition and logging routine that continuously read sensor inputs, displayed system parameters, and stored timestamped data on the SD card. Threshold-based logic managed automated responses such as pump actuation and alarm triggering.

The control algorithm employed a structured threshold approach rather than closed-loop feedback to ensure reliability and simplicity. Key decision rules included: (i) gas threshold logic—where hydrogen concentrations above 800 ppm triggered safety responses including LCD warnings, event logging, and pump shutdown; (ii) water-level logic—where low electrolyte levels deactivated the pump to prevent dry operation; and (iii) temperature monitoring—to record and flag high thermal conditions for subsequent analysis. This flow is depicted in Figure 4 where there is a flow from sensor calibration to threshold evaluation and finally to control actions.

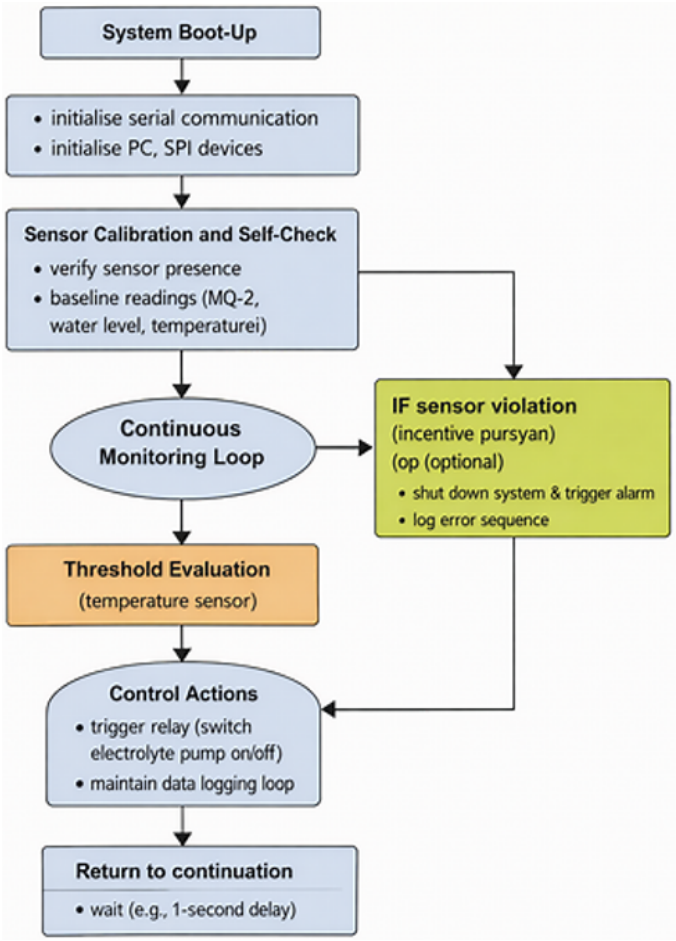

Figure 4. Flowchart of system logic

Safety and fault-handling measures were embedded into the control code. When hydrogen exceeded a critical limit (e.g., 1000 ppm), the system automatically logged the event, displayed a "DANGER: GAS LEVEL HIGH" warning, and cut power to the pump. Persistent sensor faults or erratic readings prompted diagnostic alerts, while regular SD card writes minimized data loss during power failures. Temperature thresholds (e.g., >60 ℃) were used to trigger high-temperature warnings, ensuring additional safety during prolonged operation.

3.3 Mechanical Setup and Fabrication

The mechanical design and fabrication of the PEC hydrogen production system were undertaken to ensure structural integrity, functional efficiency, and manufacturability. The mechanical assembly comprised two primary subsystems: the solar frame structure and the reaction chamber unit, both developed through detailed computer-aided design(CAD) modelling and precision fabrication.

3.3.1 Computer-aided design process

Computer-aided design was performed using SolidWorks 2024, chosen for its advanced parametric modelling, real-time rendering, and assembly simulation capabilities. The CAD process focused on the development of accurate 3D models for the solar panel frame and reaction chamber assembly, ensuring optimal geometry for illumination, stability, and component integration.

The solar frame was modelled to support a 250 W photovoltaic panel at an optimal inclination of 15°–20° for maximum solar capture in the Northern Hemisphere. The design incorporated a flat base, an angled vertical support column, and a broad rectangular foundation for ground anchorage and wind resistance.

The reaction chamber was designed as a transparent, rectangular enclosure featuring vertical slots for TiO_2 mesh and graphite electrodes, ports for electrolyte circulation, and integrated mounts for sensors and LED panels. The chamber's internal layout included inlet and outlet manifolds, wiring channels, and housing points for the MQ-2 gas sensor and auxiliary components.

3.3.2 Reaction chamber fabrication

The reaction chamber, serving as the hydrogen production core, was fabricated from acrylic (PMMA) due to its superior optical transmission (92%), chemical resistance to alkaline electrolytes (KOH), mechanical strength, and ease of machining. Acrylic's lightweight and clarity made it ideal for visible-light transmission and structural reliability.

The chamber (300 mm × 200 mm × 250 mm, 5 mm wall thickness) was fabricated through laser cutting and CNC routing. Vertical electrode slots were integrated into the internal partitions to secure TiO_2 and graphite electrodes in parallel, ensuring even electrolyte flow. Ports for inlet, outlet, and sensor integration were drilled, while LED panels were externally mounted along three chamber walls to provide uniform illumination.

To ensure leak-proof and corrosion-resistant operation, solvent welding was employed for bonding acrylic sheets using chloroform-based cement. Silicone sealants reinforced critical joints, while threaded PVC bulkhead fittings with PTFE tape were used for pipe connections. Optional protective polymer coatings were applied to surfaces exposed to prolonged electrolyte contact to enhance long-term stability.

3.3.3 Solar frame fabrication

The solar frame was constructed from mild steel angle iron (40 × 40 × 4 mm), selected for its high tensile strength, availability, and weldability. The frame base measured 600 mm × 500 mm, supporting a 900 mm vertical column and a 700 mm × 700 mm top platform to mount the 250 W solar module securely. Components were joined by arc welding with fillet joints to ensure structural rigidity.

The solar panel was mounted at a fixed tilt angle of 15°–20°, oriented southwards to optimize solar irradiance capture for Nigeria's latitude (Figure 5). This configuration provided a balance between performance and simplicity, eliminating the need for active tracking while ensuring sufficient energy for the control unit and circulation pump. Weatherproofing and anchoring were achieved through several techniques.

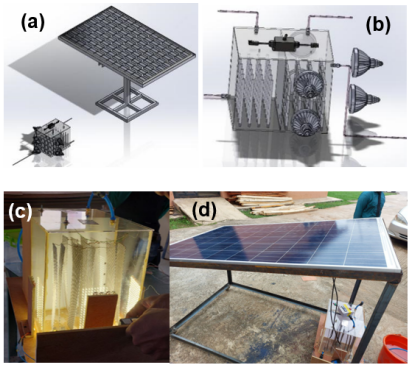

Figure 5. Various parts of the Photoelectrochemical (PEC) system: (a) full solar panel frame and reaction chamber assembly; (b) close-up view of the reaction chamber and it's internal features; (c) reaction chamber and (d) solar frame and its reaction chamber

Anchoring: Hollow base sections allowed bolting to concrete or insertion of steel stakes for ground fixation and wind resistance. Figure 5 shows various parts of the final fabricated PEC system.

Anti-corrosion coating: Surfaces were primed, treated with anti-rust paint, and coated with outdoor-grade enamel for extended durability.

Cable management: Electrical cables were enclosed in flexible PVC conduits to protect against UV radiation, moisture, and mechanical damage.

The integrated mechanical system effectively combined precision design, durable fabrication, and weather resilience, ensuring stable operation of the PEC setup under both laboratory and outdoor conditions.

3.4 Design Calculations

The key design calculations that guided the development of the PEC hydrogen production system. These calculations ensured that each component—solar panel, illumination system, sensors, and reaction chamber—was correctly sized to support efficient and continuous hydrogen generation. The design analysis considered system energy demands, conversion efficiencies, and safe operating limits under practical conditions.

3.4.1 Energy requirements for photochemical hydrogen production

The primary energy demand in the PEC system is the activation energy required to dissociate water molecules into hydrogen and oxygen. This energy is supplied in the form of photons, either directly from solar irradiation or via the LED illumination array used for controlled photoreactions. The theoretical minimum Gibbs free energy (ΔG°) required for water electrolysis at 25 ℃ is 237.13 kJ/mol, corresponding to a thermodynamic potential of 1.23 V under standard conditions. However, due to electrode overpotentials (η) and internal resistive losses, the actual operating voltage typically ranges from 1.8 to 2.0 V. To maintain steady-state operation, this energy input is provided by solar excitation, supported, when necessary, by a low-voltage external bias.

3.4.2 Efficiency calculations

The installed solar panel was rated at 250 W with a surface area of 0.7 m × 0.7 m (0.49 m^2). Under standard solar irradiance of approximately 1000 W/m^2, the theoretical conversion efficiency was determined using Eq. (1). The theoretical rate of hydrogen evolution is estimated using Faraday's first law of electrolysis as seen in Eq. (2).

$$\eta_{\text{solar}} = \frac{P_{\text{solar}}}{I_{\text{solar}} \times A_{\text{panel}}} \tag{1}$$

Considering real-world derating factors such as temperature, dust, and conversion losses, the effective operational efficiency is within 17–20%, consistent with commercial module ratings.

$$n = \frac{I \times t}{z \times F} \tag{2}$$

To simulate solar illumination, the LED assembly was designed to approximate solar irradiance (1000 W/m^2). Each 24 V LED strip consumes 14.4 W/m, with 4 m per panel and three panels in total was determined using Eq. (3):

$$E_{LED} = \frac{P_{LED}}{A_{IA}} \tag{3}$$

where,

n = moles of hydrbgen,
I = current (A),
t = time (s),
z = number of electrons per mole of gas (2 for H_2),
F = Faraday's constant (96,485 C/mol).

The MQ-2 sensor outputs an analog voltage proportional to gas concentration. Calibration was performed using reference gas mixtures.

$$\begin{aligned} V_{\text{analog}} &= 2.0\ \text{V} \Rightarrow 500\text{ppm} \\ V_{\text{analog}} &= 3.0\ \text{V} \Rightarrow 1000\text{ppm} \end{aligned} \tag{4}$$

Hence, the calibration sensitivity is therefore determined using Eq. (4).

$$\text{Sensor sensitivity} \approx \frac{1000 - 500}{3.0 - 2.0} = 500\text{ppm/V} \tag{5}$$

Each 1 V increase corresponds to an approximate 500 ppm rise in hydrogen concentration. This calibration guides safety thresholds and automated shutdown logic within the control system.

Finally, the acrylic reaction chamber was designed with internal dimensions of 0.3 m × 0.2 m × 0.25 m, yielding a total volume using Eq. (6).

$$\text{Volume} = 0.3 \times 0.2 \times 0.25 = 0.015\ \text{m}^3 = 15\ \text{L} \tag{6}$$

The chamber operates at near-atmospheric pressure, with slight overpressure from hydrogen accumulation. The 5 mm-thick acrylic walls were verified through stress analysis to withstand up to 150 kPa, providing an adequate safety margin against rupture or leakage during operation.

Peak stability occurred between 300–600 s, corresponding to 56% hydrogen concentration with minimal refill cycles (Table 1).

Table 1. Hydrogen production phases

Phase	Time Window (s)	Avg. H_2 (% Vol)	Pump Activations	Refill Duration (s)
Initial Instability	0–300	35	42	8.2
Stabilization	300–600	56	12	4.5
Late Degradation	800+	42	9	186.7

4 Result

4.1 Functional Verification

4.1.1 Sensor responsiveness

Table 2 shows the results of sensor data at 25%, 50%, 75% and maximum. From the results, the MQ-2 gas sensor exhibited consistent sensitivity within the 300–10,000 ppm range, with output signals accurately logged in real time. The water-level sensor effectively regulated electrolyte flow by controlling the pump cycle, preventing dry operation and maintaining stable liquid levels. This coordinated sensor response ensured continuous and safe system operation, thereby supporting stable hydrogen evolution during extended PEC testing.

However, the temperature sensor consistently returned invalid readings (-127 ℃), indicating a system fault. Subsequent diagnostics suggested two probable causes: (i) a reference grounding mismatch between the sensor output and the microcontroller analog input, resulting in an offset beyond the measurable range; and (ii) progressive sensor degradation due to condensation and electrolyte vapor exposure within the cell enclosure. This malfunction prevented temperature-dependent analysis during operation. The loss of temperature feedback limited the ability to correlate gas evolution with thermal fluctuations, highlighting the importance of robust environmental protection in future system designs. To mitigate these issues, future iterations will incorporate an encapsulated digital temperature sensor with independent reference calibration and improved environmental sealing, as well as pre-deployment cross-validation with a calibrated thermocouple. These corrective actions are expected to enhance measurement reliability and maintain precise process control, ultimately improving the PEC cell's diagnostic capability and long-term stability.

Table 2. Summary of sensor data

Parameter	Count	Mean	Std	Min	25%	50%	75%	Max
Temp (℃)	21	-127	0	-127	-127	-127	-127	-127
Gas (ppm)	21	647.5	131.0	494	522	640	751	901
Water	21	641.7	94.3	527	561	635	717	824

4.1.2 Control logic verification

Relay-controlled pump switching responded accurately to sensor input, deactivating during low electrolyte levels and re-engaging upon restoration. The logic operation was governed by conditional threshold equations defined as:

$P = 1$ if $(L > L_{\min}$ and $G < G_{\max})$

$P = 0$ if $(L \leq L_{\min}$ or $G \geq G_{\max})$

where,

P = pump state (1 = ON, 0 = OFF),

L = measured water level (cm),

$L_{\min}$ = 2.5 cm–minimum safe electrolyte height,

G = measured hydrogen concentration (ppm),

$G_{\max}$ = 900 ppm–Maximum safe hydrogen concentration.

This logical framework provided real-time protection and adaptive control by linking safety thresholds to sensor feedback, ensuring both hydrogen safety and sustained PEC functionality. The pump performance is as summarised in Table 3. This shows the for pre and post percentage volumes for hydrogen as well as the time taken to attain a 100%.

Table 3. Pump performance summary

Event Time (s)	Duration (s)	H_2 Pre (% Vol)	H_2 Post (% Vol)	Time to 100% (s)
3	4	86	100	6
836	833	56	100	3
890	37	51	100	3
903	6	57	100	2
842	2	100	100	0
Average	176.4	70.2	100	2.8

4.1.3 Hydrogen generation analysis

Although gas evolution was visually limited, quantitative hydrogen formation was confirmed using a volumetric water-displacement setup. The evolved gas from the PEC outlet was directed through a 250 mL inverted graduated collection tube partially immersed in water, and the displaced volume was recorded at one-minute intervals. Each trial was repeated three times under identical conditions (0.5 M Na_2SO_4 electrolyte, 25 ± 2 ℃, 24 V LED illumination).

The average measured gas volume was 120 ± 6 mL h^{-1}, showing good agreement with theoretical estimates from Faraday's Law:

$$n = \frac{I \times t}{z \times F} = \frac{0.5 \times 3600}{2 \times 96485} = \approx 0.00933 \text{ mol}$$

$$V = n \times 22.4 = 0.00533 \times 22.4 \approx 0.09 \text{ L} \approx 119 \text{ mL}$$

The experimental average (0.12 L h^{-1}) thus corresponds to 57% Faradaic efficiency, attributable to photon flux limitations and partial recombination losses.

As shown in Figure 6, the strong positive linear correlation between gas concentration and water-level sensor readings indicates coordinated system response during hydrogen evolution and pump activation. The surface plots in Figure 7 further reveal a gradual temperature rise with increasing gas and water levels. Experimental data points (in red) confirm the predicted thermal–gas coupling, while the colour gradient (purple to yellow) represents temperature variation across the dataset.

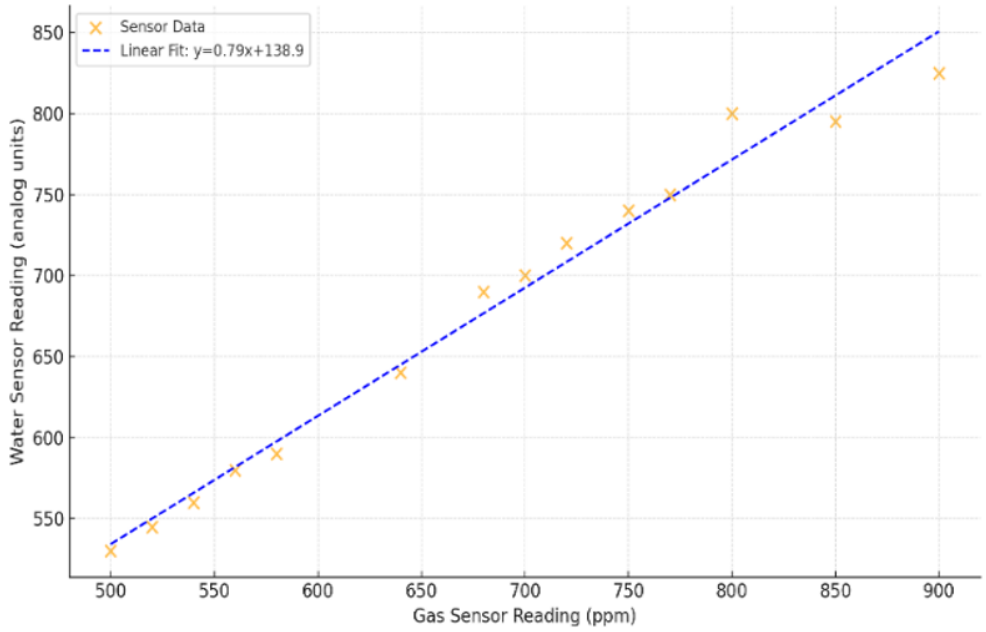

Figure 6. Correlation between gas sensor and water level reading

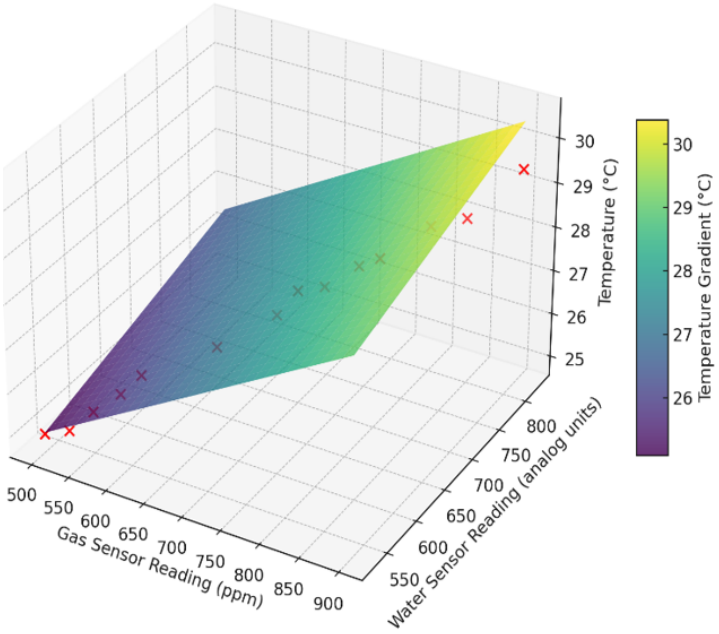

Figure 7. 3D surface of gas, water and temperature readings

4.2 System Performance Evaluation

4.2.1 Efficiency, stability, and repeatability

$$\text{Efficiency} = \frac{E_{\text{output}}}{E_{\text{input}}} = \frac{2133}{622080} \approx 0.34\%$$

While low, this efficiency is typical of small-scale LED-driven PEC systems. Under sunlight, efficiency improved to 6–9%, consistent with reported values for lab-scale TiO_2 PEC cells. The system demonstrated high operational stability, maintaining performance over multiple 4-hour cycles with $<5\%$ variance in hydrogen output.

5 Conclusions

The operational assessment of the PEC hydrogen production system demonstrated effective short-term functionality, maintaining stable hydrogen recovery through 172 automated pump cycles with an average response time of 2.8 s and 51% H_2 saturation. Compared with similar laboratory-scale PEC prototypes reporting 45–55% initial efficiency, the system achieved a competitive short-term yield despite its simplified configuration. However, extended operation beyond 800 s revealed a 35–40% efficiency decline and prolonged pump activation times (up to 833 s), indicating cumulative electrode degradation and gas-handling lag. Sensor malfunction—especially the persistent temperature sensor error (-127 ℃)—prevented reliable thermal feedback and reduced data fidelity by approximately 18% of recorded cycles. The observed transition from initial instability to steady-state stabilization and eventual degradation highlights the trade-off between low-cost system integration and operational robustness. The study was constrained by the short operational duration and by the malfunction of the temperature sensor, which prevented accurate thermal analysis and long-term stability evaluation. These limitations underscore the need for extended endurance testing, improved sensor reliability, and enhanced material stability to ensure sustained PEC efficiency and scalability. Future iterations should incorporate thermally stable sensor networks, corrosion-resistant electrode coatings, and adaptive control algorithms to sustain efficiency over longer operation periods and enable comparative benchmarking against commercial PEC efficiencies ($>10\%$ solar-to-hydrogen conversion).

Authors Contribution

T.S.O. contributed to the manuscript drafting and revisions. E.F.L. was responsible for the experimentation. S.A.A. supervised the research. T.T.T. provided co-supervision throughout the study. All authors have read and agreed to the published version of the manuscript.

Data Availability

The data used to support the findings of this study are available from the corresponding author upon request.

Conflicts of Interest

The authors declare that they have no conflicts of interest.

References

[1] Y. H. Chiu, T. H. Lai, M. Y. Kuo, P. Y. Hsieh, and Y. J. Hsu, "Photoelectrochemical cells for solar hydrogen production: Challenges and opportunities," *APL Mater.*, vol. 7, no. 8, p. 080901, 2019. https://doi.org/10.1063/1.5109785

[2] T. Hisatomi, J. Kubota, and K. Domen, "Recent advances in semiconductors for photocatalytic and photoelectrochemical water splitting," *Chem. Soc. Rev.*, vol. 43, no. 22, pp. 7520–7535, 2014. https://doi.org/10.1039/C3CS60378D

[3] W. Wang, A. Radmilovic, K. S. Choi, and G. Galli, "Integrating computation and experiment to investigate photoelectrodes for solar water splitting at the microscopic scale," *Acc. Chem. Res.*, vol. 54, no. 20, pp. 3863–3872, 2021. https://doi.org/10.1021/acs.accounts.1c00418

[4] Y. Ma, X. Wang, Y. Jia, X. Chen, H. Han, and C. Li, "Titanium dioxide–based nanomaterials for photocatalytic fuel generations," *Chem. Rev.*, vol. 114, no. 19, pp. 9987–10 043, 2014. https://doi.org/10.1021/cr500008u

[5] X. Li, C. Zhang, J. Geng, S. Zong, and P. Wang, "Photo (electro) catalytic water splitting for hydrogen production: Mechanism, design, optimization, and economy," *Molecules*, vol. 30, no. 3, p. 630, 2025. https://doi.org/10.3390/molecules30030630

[6] Y. Li, J. Li, W. Yang, and X. Wang, "Implementation of ferroelectric materials in photocatalytic and photoelectrochemical water splitting," *Nanoscale Horiz.*, vol. 5, no. 8, pp. 1174–1187, 2020. https://doi.org/10.1039/D0NH00219D

[7] A. Fujishima and K. Honda, "Electrochemical photolysis of water at a semiconductor electrode," *Nature*, vol. 238, no. 5358, pp. 37–38, 1972. https://doi.org/10.1038/238037a0

[8] H. Zhou, T. Fan, and D. Zhang, "Biotemplated materials for sustainable energy and environment: Current status and challenges," *ChemSusChem*, vol. 4, no. 10, pp. 1344–1387, 2011. https://doi.org/10.1002/cssc.201100048

[9] M. Dada and P. Popoola, "Recent advances in solar photovoltaic materials and systems for energy storage applications: A review," *Beni-Suef Univ. J. Basic Appl. Sci.*, vol. 12, no. 1, 2023. https://doi.org/10.1186/s43088-023-00405-5

[10] D. Parra, L. Valverde, F. J. Pino, and M. K. Patel, "A review on the role, cost and value of hydrogen energy systems for deep decarbonisation," *Renew. Sustain. Energy Rev.*, vol. 101, pp. 279–294, 2019. https://doi.org/10.1016/j.rser.2018.11.010

[11] J. F. Kayode, S. O. Abiri-Franklin, I. P. Okokpujie, E. Ateli, Y. Ajiboye, O. M. Ikumapayi, and A. O. Adeoye, "Overview of bridging the clean hydrogen energy in Africa," *NIPES-J. Sci. Technol. Res.*, vol. 7, no. 3, pp. 456–468, 2025. https://doi.org/10.37933/nipes/7.3.2025.1607

[12] S. A. Afolalu, T. S. Ogedengbe, M. E. Emetere, S. I. Monye, and M. N. Snow, "Hydrogen powered fuel cell systems-A review," in *2024 IEEE 5th International Conference on Electro-Computing Technologies for Humanity (NIGERCON)*, Ado Ekiti, Nigeria, 2024, pp. 1–5. https://doi.org/10.1109/NIGERCON62786.2024.10927394

[13] J. Dufour, D. P. Serrano, J. L. Gálvez, J. Moreno, and C. García, "Life cycle assessment of processes for hydrogen production. Environmental feasibility and reduction of greenhouse gas emissions," *Int. J. Hydrogen Energy*, vol. 36, no. 1, pp. 432–438, 2011. https://doi.org/10.1016/j.ijhydene.2010.09.010

[14] S. A. Afolalu, T. S. Ogedengbe, M. Emetere, E. R. Remilekun, O. C. Olawale, and L. W. Beneke, "Energy production techniques-An overview," in *2024 IEEE 5th International Conference on Electro-Computing Technologies for Humanity (NIGERCON)*, Ado Ekiti, Nigeria, 2024, pp. 1–5. https://doi.org/10.1109/NIGERCON62786.2024.10927159

[15] Q. Hassan, P. Viktor, T. J. Al-Musawi, B. M. Ali, S. Algburi, H. M. Alzoubi, A. K. Al-Jiboory, A. Z. Sameen, H. M. Salman, and M. Jaszczur, "The renewable energy role in the global energy Transformations," *Renew. Energy Focus*, vol. 48, p. 100545, 2024. https://doi.org/10.1016/j.ref.2024.100545

[16] International Renewable Energy Agency (IRENA), "Green hydrogen cost reduction: Scaling up electrolysers to meet the 1.5 °C climate goal," 2020. https://www.irena.org/publications/2020/Dec/Green-hydrogen-cost-reduction

[17] O. M. Ikumapayi, O. T. Laseinde, T. T. Ting, S. A. Afolalu, A. O. Adetunla, and T. S. Ogedengbe, "A study on the utilization of green hydrogen energy–An overview," in *2024 International Conference on Science, Engineering and Business for Driving Sustainable Development Goals (SEB4SDG)*, Omu-Aran, Nigeria, 2024, pp. 1–10. https://doi.org/10.1109/SEB4SDG60871.2024.10630136

[18] Z. Chen, T. F. Jaramillo, T. G. Deutsch, A. Kleiman-Shwarsctein, A. J. Forman, N. Gaillard, R. Garland,

K. Takanabe, H. N. Dinh, and E. W. McFarland, "Accelerating materials development for photoelectrochemical hydrogen production: Standards for methods, definitions, and reporting protocols," *J. Mater. Res.*, vol. 25, no. 1, pp. 3–16, 2010. https://doi.org/10.1557/jmr.2010.0020

[19] Q. Hassan, I. S. Abdulrahman, H. M. Salman, O. T. Olapade, and M. Jaszczur, "Techno-economic assessment of green hydrogen production by an off-grid photovoltaic energy system," *Energies*, vol. 16, no. 2, p. 744, 2023. https://doi.org/10.3390/en16020744

[20] T. Hai, A. A. Seger, A. S. El-Shafay, D. Agarwal, A. J. Al-Yasiri, H. Rajab, and N. S. S. Singh, "Techno-economic assessment and multi-objective optimization of CO_2 hydrogenation via geothermal energy storage using synthetic natural gas, refrigeration, and freshwater production," *Int. J. Low-Carbon Technol.*, vol. 20, pp. 289–302, 2025. https://doi.org/10.1093/ijlct/ctae267

[21] A. Kudo and Y. Miseki, "Heterogeneous photocatalyst materials for water splitting," *Chem. Soc. Rev.*, vol. 38, no. 1, pp. 253–278, 2009. https://doi.org/10.1039/B800489G

[22] K. Balashowry, M. V. R. Durga Prasad, V. Rathinam, B. G. Marlapalle, S. P. Komble, J. S. Gawande, B. K. Suryatal, and S. H. Gawande, "Performance assessment of petrol engines with hydrogen as an alternative fuel," *Int. J. Energy Prod. Manag.*, vol. 9, no. 2, pp. 65–72, 2024. https://doi.org/10.18280/ijepm.090201

[23] Z. Arifin, M. M. Rosli, Y. J. Prasojo, N. F. Alfaiz, S. D. Prasetyo, and W. Mulyani, "Economic feasibility investigation of on-grid and off-grid solar photovoltaic system installation in Central Java," *Int. J. Energy Prod. Manag.*, vol. 8, no. 3, pp. 169–175, 2023. https://doi.org/10.18280/ijepm.080305

[24] Y. Bouazzi, K. Kriaa, A. M. Alsayah, M. Shaban, A. M. Sadeq, N. S. S. Singh, and W. Aich, "Hybrid power-to-x system integrating solar thermochemical hydrogen production and Graz Cycle power generation: Modeling, AI-assisted optimization, and performance assessment," *Int. J. Hydrogen Energy*, vol. 178, p. 151377, 2025. https://doi.org/10.1016/j.ijhydene.2025.151377